



RESEARCH ARTICLE

10.1029/2023JG007590

Key Points:

- Active floodplains in the Lena River Delta contain sandy permafrost soils with strongly varying C stocks despite similar surface vegetation
- Carbon stocks in active floodplains were relatively low but only 40% was found in surface soils indicating the importance of deep soils
- Potential carbon loss from incubations showed average aerobic carbon production but very active anaerobic carbon and methane production

Supporting Information:

Supporting Information may be found in the online version of this article.

Correspondence to:

C. C. Treat,
claire.treat@awi.de

Citation:

Herbst, T., Fuchs, M., Liebner, S., & Treat, C. C. (2024). Carbon stocks and potential greenhouse gas production of permafrost-affected active floodplains in the Lena River Delta. *Journal of Geophysical Research: Biogeosciences*, 129, e2023JG007590. <https://doi.org/10.1029/2023JG007590>

Received 23 MAY 2023

Accepted 5 DEC 2023

Author Contributions:

Conceptualization: Tanja Herbst, Matthias Fuchs, Claire C. Treat

Data curation: Tanja Herbst, Matthias Fuchs, Claire C. Treat

Formal analysis: Tanja Herbst, Claire C. Treat

Investigation: Tanja Herbst, Matthias Fuchs, Claire C. Treat

Methodology: Tanja Herbst, Matthias Fuchs, Susanne Liebner, Claire C. Treat

Resources: Susanne Liebner, Claire C. Treat

© 2024. The Authors.

This is an open access article under the terms of the [Creative Commons Attribution-NonCommercial-NoDerivs License](https://creativecommons.org/licenses/by-nc-nd/4.0/), which permits use and distribution in any medium, provided the original work is properly cited, the use is non-commercial and no modifications or adaptations are made.

Carbon Stocks and Potential Greenhouse Gas Production of Permafrost-Affected Active Floodplains in the Lena River Delta

Tanja Herbst¹, Matthias Fuchs^{2,3} , Susanne Liebner⁴ , and Claire C. Treat² 

¹Faculty of Environment and Natural Resources, Albert-Ludwigs-University, Freiburg, Germany, ²Alfred Wegener Institute Helmholtz Center for Polar and Marine Research, Potsdam, Germany, ³Now at Institute of Arctic and Alpine Research, University of Colorado Boulder, Boulder, CO, USA, ⁴Helmholtz-Zentrum Potsdam Deutsches GeoForschungsZentrum GFZ, Potsdam, Germany

Abstract Arctic warming increases the degradation of permafrost soils but little is known about floodplain soils in the permafrost region. This study quantifies soil organic carbon (SOC) and soil nitrogen stocks, and the potential CH₄ and CO₂ production from seven cores in the active floodplains in the Lena River Delta, Russia. The soils were sandy but highly heterogeneous, containing deep, organic rich deposits with >60% SOC stored below 30 cm. The mean SOC stocks in the top 1 m were 12.9 ± 6.0 kg C m⁻². Grain size analysis and radiocarbon ages indicated highly dynamic environments with sediment re-working. Potential CH₄ and CO₂ production from active floodplains was assessed using a 1-year incubation at 20°C under aerobic and anaerobic conditions. Cumulative aerobic CO₂ production mineralized a mean 4.6 ± 2.8% of initial SOC. The mean cumulative aerobic:anaerobic C production ratio was 2.3 ± 0.9. Anaerobic CH₄ production comprised 50 ± 9% of anaerobic C mineralization; rates were comparable or exceeded those for permafrost region organic soils. Potential C production from the incubations was correlated with total organic carbon and varied strongly over space (among cores) and depth (active layer vs. permafrost). This study provides valuable information on the carbon cycle dynamics from active floodplains in the Lena River Delta and highlights the key spatial variability, both among sites and with depth, and the need to include these dynamic permafrost environments in future estimates of the permafrost carbon-climate feedback.

Plain Language Summary Floodplain soil development results from both geological processes, such as sediment erosion and deposition, and biological processes such as vegetation growth. In the Arctic, these processes interact with permafrost to form deep soils, but the carbon stocks and potential decomposition and greenhouse gas emissions from Arctic floodplain soils are relatively unknown. In this study, we investigate carbon stocks and potential decomposition from Arctic floodplain soils to depths of 1 m from a large river delta in Siberia. We show that it is difficult to predict what soil types, carbon stocks, and potential decomposition and emissions are found beneath the surface because the sites vary strongly despite having similar vegetation at the surface owing to the depositional processes that occur in floodplains.

1. Introduction

The Arctic is currently warming much faster than the rest of the globe (Rantanen et al., 2022). Northern high latitude ecosystems are exposed to drastic changes, which also has an impact on the widespread permafrost soils in these regions (Obu et al., 2019). Permafrost is defined as ground that remains at or below 0°C for two or more consecutive years (Harris et al., 1988). As the frozen state of these soils prevents decomposition processes, permafrost has been accumulating undecomposed organic matter since the end of the last ice age or longer (J. W. Harden et al., 1992; Schirmer et al., 2002; Zimov et al., 2006). It is estimated that northern permafrost regions store ~1,300 Pg of soil carbon (Hugelius et al., 2014), which is about half of the globally stored soil organic carbon (SOC) (Köchy et al., 2015). With climate warming, permafrost soils are warming and thawing (Biskaborn et al., 2019), potentially increasing the decomposition of previously frozen organic material, which can be released to the atmosphere either as CO₂ or as CH₄ and further enhancing climate warming (Schuur et al., 2015).

Many studies of C stocks in permafrost soils mention a poorly described stock of deep permafrost deposits: Arctic river deltas (Hugelius et al., 2014; Overeem et al., 2022). The major Arctic river deltas in permafrost regions

Supervision: Matthias Fuchs, Claire C. Treat

Writing – original draft: Tanja Herbst, Matthias Fuchs, Claire C. Treat

Writing – review & editing: Tanja Herbst, Matthias Fuchs, Susanne Liebner, Claire C. Treat

occupy only 77,000 km² (Walker, 1998), but play an important role as carbon stocks. Delta sediment deposits can have a large thickness of up to 60 m due to typical river deltaic sedimentation and accumulation processes (Schwamborn et al., 2002). Moreover, these are highly dynamic environments at the land-sea interface, characterized by active fluvial, coastal, deltaic, and permafrost-thaw processes including periodic flooding, sediment deposition, erosion (Overeem et al., 2022), which impact the soil carbon (C) and nitrogen (N) stocks (Fuchs et al., 2018b). However, as these processes differ from other soil forming processes in the permafrost regions such as peat deposition, yedoma deposition, and cryoturbation, it is unclear how permafrost C stocks in these soils compare with others (Harden et al., 2012; Hugelius et al., 2014).

Active floodplains in Arctic river deltas are highly dynamic due to active erosion and sedimentation by annual spring flooding (Zubrzycki et al., 2013) but they remain understudied, despite being the dominant unit in many Arctic river deltas. Active floodplains consist of sand-rich soils and are expected to not store as large amounts of organic carbon as other geomorphological terraces of the delta (Siewert et al., 2016). Only a few studies have focused on C and N stocks and greenhouse gas release from active floodplains within Arctic river deltas. Zubrzycki et al. (2013) studied the SOC and soil nitrogen (SN) stocks and pools of the active floodplains on Samoylov Island in the Lena Delta and Siewert et al. (2016) included alluvial sediments and active floodplains on Kurungnakh Island in the Lena Delta in their study. Further C and N stocks were quantified in deltaic deposits in Alaska (Fuchs et al., 2018b; Ping et al., 2011) and Siberia (Hugelius et al., 2013, 2014). There are also few studies on greenhouse gas emissions from active floodplains. One study from Siberia showed substantially higher CH₄ fluxes in the active floodplains compared to drier sites (van Huissteden et al., 2005), highlighting the potential of high CH₄ production and emission from active floodplains. Similarly, in an incubation study using soils from Arctic Siberia, potential CH₄ production was highest in a floodplain core relative to upland yedoma samples (Laurent et al., 2023). These large uncertainties and limited data about C cycling in active floodplains but potentially high production and emission of CH₄ warrant further quantification of carbon stocks and potential CO₂ and CH₄ production from these dynamic permafrost areas.

In this study, soil cores including active layer and permafrost layer of active floodplains in the Lena Delta were analyzed with the aim (a) to determine SOC and SN stocks down to 1 m depth and (b) to investigate the potential CO₂ and CH₄ production of active floodplain soils under aerobic and anaerobic conditions. The underlying hypotheses were: the soils are sand-rich and store less organic carbon than other landscape units in the Lena Delta, the active floodplain soils are comparatively young and sedimentation rates are high due to periodic flooding, and emissions are related to soil characteristics (e.g., soil carbon, C/N, and water content). We analyzed key soil properties, such as pH, conductivity, total organic carbon (TOC), total nitrogen (TN), C/N ratio, bulk density, water content, grain size, and radiocarbon ages and conducted a year-long laboratory incubation of active and permafrost layer samples in order to gain a better understanding of the C accumulation, C stocks and potential C production from the active floodplains in the Lena Delta.

2. Materials and Methods

2.1. Study Area and Soil Sampling

The study area is located in the northeastern Siberian Lena River Delta within the continuous permafrost zone in northern Yakutia. The Lena Delta is the largest delta in the Arctic (Boike et al., 2013). The region has an Arctic continental climate with low temperatures and low precipitation (Boike et al., 2019). The mean annual air temperature at Samoylov research station from 1998 to 2011 was -12.5°C , with mean annual rainfall of 125 mm (Boike et al., 2013).

The Lena Delta can be classified into three main geomorphological, terrace-like units and the modern floodplains (Schwamborn et al., 2002). The floodplains and the youngest unit are of Holocene origin and are characterized by polygonal wet tundra with ice wedges and large thermokarst lakes overlying organic-rich sands with silty-sandy peat layers (Schwamborn et al., 2002). The soil cores analyzed in this study are from the active floodplains on Kurungnakh, Samoylov Island, and the neighboring island Khongordokh-Ary in the southern part of the Lena Delta (Figure 1). Kurungnakh Island ($72^{\circ}20'\text{N}$; $126^{\circ}18'\text{E}$) is composed of Late Quaternary sediments. The soil cores analyzed here from Kurungnakh belong to the small active floodplain in the eastern part of the island, which is similar to the cores collected in the floodplains of Samoylov Island and Khongordokh-Ary. Samoylov Island ($72^{\circ}22'\text{N}$, $126^{\circ}28'\text{E}$) is split into the Holocene river terrace and the active floodplain. The western part of

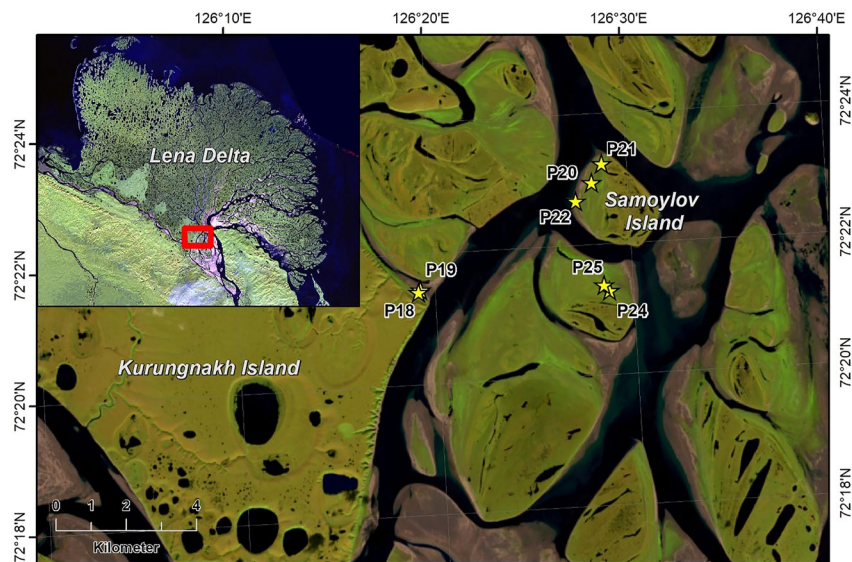


Figure 1. Location of the Lena Delta and the study sites on Kurungnakh Island (P18, P19), Samoylov Island (P20, P21, P22), and Khongordokh-Ary (P24, P25) with the corresponding soil cores. (Top right inlay: Landsat 5TM mosaic (image acquisitions 2009 and 2010), main image: Landsat 8 image—acquisition date 23 August 2016, image courtesy of the U.S. Geological Survey).

Samoylov Island consists of the active floodplains, which are either non-vegetated or with dwarf shrubs dominated tundra (Boike et al., 2019; Siewert et al., 2016) with an altitude of up to 5 m a.s.l. Khongordokh-Ary is also part of the active floodplain, which is affected by fluvial sedimentation and is flooded at least once in spring and during high river water levels (Zubrzycki et al., 2013). Overall, active floodplains cover 8,830 km² of land area in the Lena River Delta (Zubrzycki et al., 2013).

The soil coring and sampling was carried out in August 2018 (Kruse et al., 2019). First, vegetation and other characteristics of the plots were described (Table 1). Soil cores were described in the field according to their macroscopic sediment characteristic, lithology, and present plant macrofossils. In addition, we described the cryostratigraphy (ice distribution within cores) according to French and Shur (2010). Active layer soils were excavated, described, and sampled with a fixed volume cylinder (250 cm³). Next, the permafrost layers were sampled with a modified, snow, ice, and permafrost (SIPRE) auger (Jon Holmgren's Machine Shop, Fairbanks, AK, USA) to a depth of 1 m (core diameter of 7.62 cm). Each core was divided into subsamples with 5–10 cm length increments according to its facies horizons, transported frozen to Alfred Wegener Institute in Potsdam, and stored at -20°C until analysis. Seven soil cores including P18, P19, P20, P21, P22, P24, and P25 (Figure 1) were taken during the expedition from the low-lying, annually flooded plains and were assumed to be representative of the active floodplains. A total of 48 soil samples across depths were analyzed from these 7 cores, covering a range of locations, carbon contents, grain size, moisture conditions and vegetation cover (Table 1; Figure S1 in Supporting Information S1).

2.2. Soil Characteristics

Standard soil parameters such as pH, conductivity, and water content were measured on all cores. The total carbon (TC), TOC, and TN were measured to calculate the carbon and nitrogen stocks as well as the gas production rates during incubation. Grain size and radiocarbon ages were determined to investigate accumulation processes. To split the samples for these analyses, subsamples were prepared by splitting the frozen soil samples with a cleaned hammer and chisel in a climate chamber at -4°C . One subsample was used to determine pH, conductivity, water content, grain size, TOC, TC, and TN, while another subsample was used for incubations.

Soil porewater pH and electrical conductivity were measured by thawing frozen subsamples in plastic bags at 4°C overnight before extracting the porewater using rhizon soil moisture samplers. Conductivity and pH were measured with the WTW Multi 540 (Xylem Analytics, Weilheim, Germany). Gravimetric water content was

Table 1

Descriptions of the Active Floodplain Soil Cores Analyzed in This Study Including P18, P19, P20, P21, P22, P24, P25

Core name	Location	No. samples	Core depth (cm)	Active layer depth (cm)	Soil profile description	Surface description
KUR18-P18	Kurungnakh	5	69	105	Dark and light brown sand with peat layers	Sandbank, no vegetation, driftwood
KUR18-P19	Kurungnakh	9	112	82	Silty sand/sandy silt, rooted, organic inclusions	Grasses, shrubs, <i>Equisetum</i> spp., driftwood
SAM18-P20	Samoylov	9	114.5	82	Light/dark gray sand, rooted, silty sand with organic inclusions	Shrubs, <i>Equisetum</i> spp., mosses
SAM18-P21	Samoylov	9	104.5	57	Organic rich sandy silt, rooted, sandy layers, organic inclusions	<i>Equisetum</i> spp., grasses, shrubs, mosses, driftwood
SAM18-P22	Samoylov	5	66	>100	Sand without layers	Sandbank without vegetation but some grasses
SAM18-P24	Khongordokh-Ary	8	95	54	Sandy silt, rooted, organic rich and sandy layers	Shrubs, <i>Equisetum</i> spp., sedges, mosses
SAM18-P25	Khongordokh-Ary	9	102	59	Organic rich silt with roots and sand layers	<i>Dryas</i> spp., <i>Salix</i> spp., grasses, mosses, driftwood

Note. This includes the generalized locations of sampling, the number of samples per core, the total core depth, the active layer depth, the soil, site, and vegetation description. Soil, vegetation, and site description is based on field observations. Photos of study sites and soil profiles are shown in Supporting Information S1.

determined by weighing the samples before and after the freeze-drying process to determine the water content from the water loss. Bulk density was calculated based on a best-fit regression ($n = 1,091$, $R^2 = 0.85$) predicted from the absolute water content (Figure S2 in Supporting Information S1). The relationship between absolute water content and dry bulk density was developed for permafrost samples from more than 70 deltaic and tundra study sites (Fuchs et al., 2018a; Fuchs, Lenz, et al., 2018 Figure S2 in Supporting Information S1). Bulk density could not accurately be determined on the samples of this study, because the initial volume of the sub-sample was inaccurate or unknown.

The grain size distribution of the samples was determined using a Malvern Mastersizer 3000 laser particle laser analyzer. Pre-treatment of 30 g of sub-samples include the removal of organic remnants and follow the procedure described in Fuchs et al. (2018b). For each sample, at least three replicates were measured and then averaged. The instrument gave the results in grain size classes and the corresponding volume fractions in percent (vol%). The classification was made according to DIN 4022 (sand: 0.06–2.0 mm; silt: 0.002–0.06 mm; clay: <0.002 mm). Statistics were calculated using GRADISTATv 9.1 (Blott & Pye, 2001).

Carbon and N contents of the soils were determined on freeze-dried, milled samples and measured with the C analyzer soli TOC cube and the N analyzer rapid MAX N exceed (elementar, Langensfeld, Germany). The SOC and SN stocks were calculated according to Michaelson et al. (1996). The C and nitrogen N in g cm^{-3} was calculated by multiplying the dry bulk density with the TOC and TN contents. Several samples had TOC (P22-1, P22-2) and TN concentrations below the detection limit of 0.1%. For these samples, the %C concentrations were assumed to be 0.05% for the calculation of C stocks and mean TOC content, while the %N concentration was assumed to be 0%. However, in samples with TN or TOC below detection limit, the C/N ratio was not calculated, and the corresponding samples were not included in the average C/N ratio of the active and permafrost layers. Carbon and nitrogen storages in kg m^{-2} were calculated by multiplying C or N density with the sample length in cm. Depth intervals without C or N density were extrapolated from the density of the respective overlying and underlying layers with same or similar sedimentary characteristics (based on field notes). The stocks were then summed for the reference depths of 0–30 cm and 0–100 cm.

Radiocarbon dating was performed for age determination in order to assess the carbon and sediment accumulation processes on a subset of soil cores (P19, P24, and P25 at six depths because these cores were analyzed in the incubation experiment). For this, plant remains in the freeze-dried samples were handpicked under the

microscope to select organic material deposited in situ. The plant remains were weighed and then analyzed using the Mini Carbon Dating System based on accelerator mass spectrometry at Alfred Wegener Institute in Bremerhaven (Mollenhauer et al., 2021). The radiocarbon ages were calibrated with CALIBomb software using IntCal20 calibration curve and $F^{14}C$ as reference (Reimer et al., 2020). The calibrated ages are given in calibrated years before present (cal y BP) and calibrated years Common Era.

The full sedimentological data and soil properties are available at Pangaea.de (Treat et al., 2023); the cores used in this study are P18, P19, P20, P21, P22, P24, and P25.

2.3. Potential CO_2 and CH_4 Production in Incubation Experiment

The potential production of CO_2 and CH_4 due to microbial degradation of organic matter was investigated in a 1-year incubation experiment. Material from three cores (P19, P24, and P25) were incubated under aerobic and anaerobic conditions and at two depths each, representing the active layer and the permafrost layer. The core P19 is located in the Eastern part of Kurungnakh, whereas P24 and P25 are on Khongordokh-Ary (Figure 1). The cores selected because they were sufficiently deep to capture permafrost layers, were vegetated with similar vegetation types, and showed evidence of both soil formation as well as buried horizons with higher organic content, all factors assumed to be representative for the active floodplains in this region. The samples for the active and the permafrost layer of each core were selected according to comparable depths by using the field notes and first results of the soil analysis, but had different characteristics in terms of water content, TOC, and grain size (Table S1 in Supporting Information S1).

Incubations were performed at 20°C under both aerobic and anaerobic conditions for 356 days. One sample of the active layer and one sample of the permafrost layer were incubated per core with three laboratory replicates per sample, resulting in 36 incubated soil samples (18 aerobic, 18 anaerobic). In addition, two blanks were included per treatment for the determination of zero fluxes. For preparations, subsamples from the frozen soil samples were thawed in closed plastic bags overnight at 4°C before homogenizing and weighing around 15 g into 120 ml vials. Anaerobic incubation samples were prepared in a glovebox with an anoxic atmosphere (N_2), whereas the aerobic incubation samples were prepared at ambient air. The aerobic samples were kept at field moisture conditions, whereas sterilized water was added to the anaerobic ones when water content was less than 30% to achieve soil saturation. All vials were permanently closed with airtight lids (rubber stopper and aluminum lids) to create and maintain both anoxic conditions and constant humidity. The closed vials were stored at 1°C overnight to avoid the onset of microbial activity before flushing the samples prior to the first gas concentration measurement of t_0 . Anaerobic incubations were flushed with N_2 for 3 min to remove the remaining O_2 , whereas aerobic incubations were flushed with synthetic, CO_2 -free air (20% O_2 , 80% N_2). Afterward, samples were brought to incubation temperature. Incubations were performed over 52 weeks in the dark in an incubator at a constant temperature of 20°C.

The CO_2 and CH_4 concentrations were determined by gas chromatography (7890A, Agilent Technologies, USA) at the German Research Centre for Geosciences (GFZ), Potsdam. Gases were separated on an Agilent 19095P-QO4 column and quantified with a flame ionization detector. The column temperature was 50°C and helium served as a carrier gas. Before each measurement, the rubber stopper was sterilized by flaming with 99% ethanol and 350 μL from the headspace gas were taken manually with a Hamilton gastight syringe and a sterile needle. For both incubation types, measurements were taken every second day in the first 2 weeks, once or twice per week for the first 3 months, and at longer intervals for the remainder of the 1-year incubation. When CO_2 concentration exceeded 10,000 ppm during the measurement period, the headspace was flushed with synthetic air (20% O_2 , 80% N_2) for the aerobic incubations and with N_2 for the anaerobic treatment before re-measuring the samples.

The potential CO_2 and CH_4 production rates were calculated according to Robertson et al. (1999) by using the change in headspace CO_2 and CH_4 concentration over time. First, the CO_2 and CH_4 concentrations were converted from ppm_v to mass units by applying the Ideal Gas Law and correcting for differences in headspace volume due to the soil sample volumes. Then the rate of concentration change over time was calculated using a linear regression between the nearest two measurement points. Then this was normalized by the sample dry weight and per gram soil carbon. Last, the mean of the replicates per core and layer (active and permafrost) was calculated in order to determine the potential CO_2 and CH_4 production rates. The cumulative gas production

was calculated by summing the difference in concentrations between the measurements after accounting for flushing. We did not correct for Henry's Law due to the low water contents of many of the samples (Table S1 in Supporting Information S1). While CH₄ concentrations were measured in the aerobic treatments, cumulative production over the 356-day experiment was <0.2 μg CH₄-C g DW⁻¹ and considered negligible and is not discussed further.

The incubation data set can be found at (Treat et al., 2023).

2.4. Data Analysis

For all the measured parameters, means are presented with standard deviations as error estimates. Calculations, statistical tests, and plotting were done with Microsoft Excel (version 2201), and base R version 4.2.3 (R Development Core Team, 2008). To determine correlations between soil properties as well as soil properties and C production from incubations, the non-parametric Spearman correlation coefficient was used. To analyze significant differences between the soil cores, depths, and their interaction (core by depth) in the incubation experiment, ANOVA (one-way analysis of variance, *r* command: *aov*) and a pairwise post-hoc test (Tukey Honest Significant Difference, *r* command: *TukeyHSD*) were performed. To determine correlations between mean cumulative C production and soil properties, a linear regression was used for the mean value of each core by depth sample (*n* = 6) using both production per gram weight and production rates normalized for soil C content as response variables. Tests for aerobic and anaerobic production were done separately. The tested predictor variables were TOC content, water content, nitrogen content, C/N ratio, sand (%), silt (%), clay (%), and calibrated ¹⁴C ages. These statistical tests were selected even when there was no normal distribution because of the small sample size with the assumption that the data would be normally distributed if the sample size were larger.

3. Results

3.1. Soil Characteristics

The cores used in this study were from a variety of active layer floodplains, with overlying vegetation either absent or consisting of *Equisetum* spp., shrubs, grasses, and mosses (Table 1). Permafrost was present across the cores; active layers in August 2018 ranged from 54 cm to >100 cm. At the time of sampling, many of the soil profiles had standing water at the bottom of the active layer (Figure S1 in Supporting Information S1). The soils from the active floodplains were mostly sand or silty sand, the latter being more commonly found at the surface. The grain size data showed samples were from the textural groups sand, sandy silt, or silty sand. For all 48 samples, the average percentages of sand, silt and clay were 70.8%, 26.1%, and 3.1%, respectively. Overall, the sand content ranged from 24.5% to 99.4%, the silt content was between 0.5% and 66.9%, and the clay fraction was lowest with 0%–8.6%. Cores P18 and P22 from non-vegetated sandbanks had high sand contents in all depths (Figure 2). Across all cores, the grain size distribution varied with depth and sandy or silty layers were identifiable (e.g., sandy layers in P19 at a depth of 23–47 cm and in P21 at a depth of 60–81 cm). The cores P24 and P25 showed a trend of an increasing sand fraction and a decreasing silt fraction with depth (Figure 2). The water content ranged between 8% and 47%, and the dry bulk density ranged between 0.64 g cm⁻³ and 1.64 g cm⁻³ and was on average 1.07 ± 0.24 g cm⁻³.

Across the active floodplain samples, the TOC content ranged from <0.1% to 7.4% with an average of 1.68 ± 1.55% for all samples. The sand bank cores P18 and P22 had on average the lowest TOC values, sometimes below detection limit, whereas the active layer of P24 and P25 had the highest TOC (Table 2). Many of the cores from the active floodplain generally had more organic-rich layers (TOC content >2%) at the top and buried in the profile (Figure 3), while only core P24 and P25 cores showed the often observed decrease in C with depth. The TOC content was correlated with the soil texture; when the silt fraction increased, the water content and TOC also increased (Figure 3). Overall, the TN contents were very low, averaging 0.16 ± 0.06% for all samples (assuming TN = 0% when TN was below detection limit of 0.10%). Samples with TN below the detection limit occurred in all cores (Table 3; Treat et al., 2023), but all samples were below the detection limit in P18 and P22. The C/N ratio ranged from 14.4 to 24.8, with the highest ratios occurring in P24, where active and permafrost layer C/Ns averaged 22.6 ± 1.6 and 24.3 ± 0.0, respectively. The lowest ratio occurred in the permafrost layer of P19 with an average of 14.7 ± 0.2 (Table 2). Soil pH ranged from 6.85 to 7.8 with a mean of 7.3 ± 0.3 and soil conductivity ranged from 110 μS cm⁻¹ to 529 μS cm⁻¹ with the exception of two surface soil samples (914 and 1,342 μS cm⁻¹).

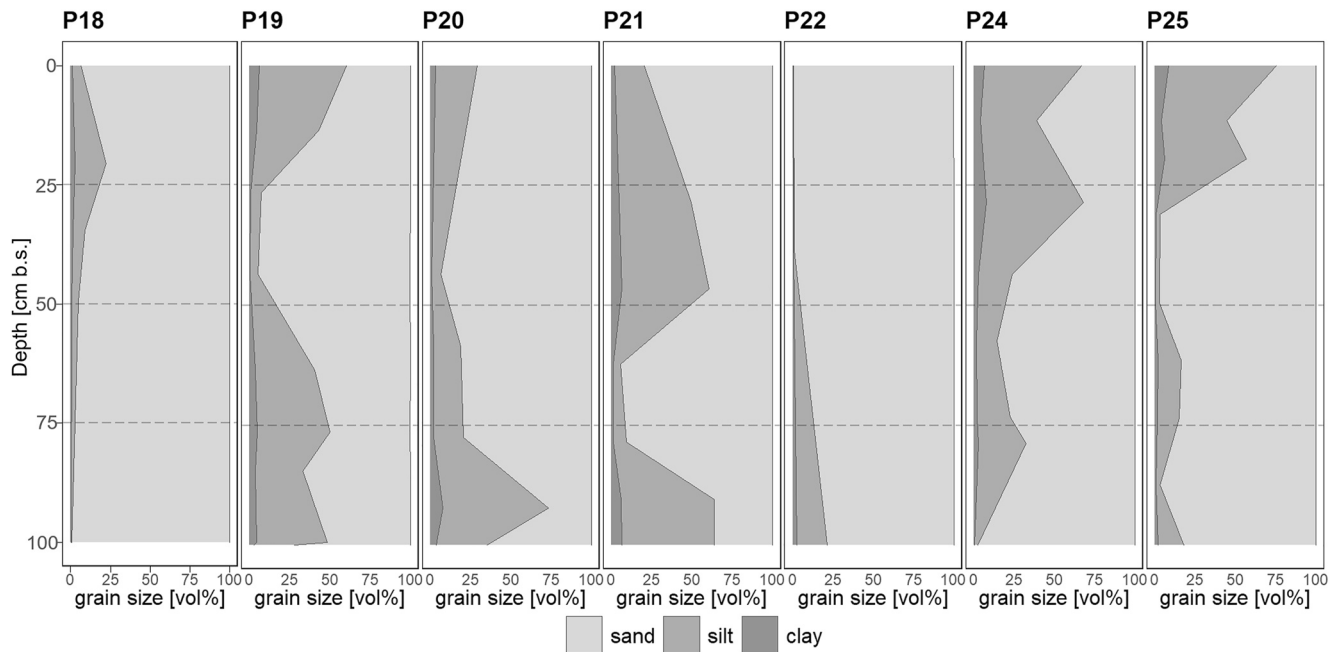


Figure 2. Grain size analysis for the seven active floodplain cores showing the relative percentages of sand, silt and clay to depths of 100 cm. Grain size analysis is interpolated between the measurement points for continuous plotting; values and depths analyzed are given in the full data set (Treat et al., 2023).

3.2. SOC and SN Stocks and Ages

In the active floodplain cores, SOC stocks for the top 1 m ranged 3.1 and 19.5 kg C m⁻² (Table 3). The mean SOC stocks across all cores were 12.89 ± 6.02 kg C m⁻². Around 40% of the C stock was stored in the first 30 cm (Table 3). The non-vegetated sandbank cores P18 and P22 had the lowest carbon stocks, while P19, P20, and P25 stored a similar amount of carbon, and P24 and P21 had the highest carbon stocks (Table 3). The nitrogen stocks of the cores were much lower, ranging from 0.61 to 1.07 kg N m⁻² (0–100 cm). The mean N stock of all cores was 0.56 ± 0.38 kg N m⁻² (0–100 cm), with 42% stored in the first 30 cm. Nitrogen stocks were not explicitly calculated for P18 and P22, because the TN contents of all their samples were below the detection limit (<0.10%) and were assumed to be 0 kg N m⁻² in averaging across the cores. By not considering the soil profiles P18 and P22 of the

Table 2

Summary of Soil Parameters for the Active Layer and Permafrost of the Analyzed Active Floodplain Cores, Given as the Mean of Active and Permafrost Layer Samples for Each Core and Corresponding Standard Deviations in Parentheses

Sample	Layer	Total depth (cm)	No. samples	pH	Conductivity (uS cm ⁻¹)	Water content (wt%)	Bulk density (g cm ⁻³)	TOC (%)	TN (%)	C/N ratio	Soil texture
KUR18-P18	Active	69	5	7.4 (0.2)	230 (90)	20 (4)	1.3 (0.1)	0.5 (0.4)	–	–	Sand, silty sand
KUR18-P19	Active	80	6	7.4 (0.4)	300 (60)	28 (7)	1.1 (0.2)	1.6 (1.0)	0.1 (0.1)	15.6 (0.9)	Sand
	Permafrost	112	3	6.9 (0.0)	270 (80)	37 (2)	0.85 (0.05)	1.5 (0.4)	0.1 (0.1)	14.7 (0.2)	Silty sand
SAM18-P20	Active	81	6	7.2 (0.1)	190 (50)	25 (5)	1.1 (0.1)	1.4 (0.6)	0.1 (0.1)	16.0 (1.3)	Sand, silty sand
	Permafrost	114.5	3	6.9 (0.0)	260 (10)	40 (8)	0.8 (0.2)	2.4 (0.9)	0.1 (0.1)	16.4 (0.1)	Sandy silt, silty sand
SAM18-P21	Active	50	5	7.3 (0.1)	440 (80)	34 (7)	0.9 (0.2)	2.5 (1.1)	0.1 (0.1)	16.6 (1.4)	Silty sand, sandy silt
	Permafrost	104.5	4	7.3 (0.2)	230 (100)	32 (11)	1.0 (0.3)	1.5 (1.1)	0.1 (0.1)	15.1 (0.7)	Sand, silty sand, sandy silt
SAM18-P22	Active	66	5	7.5 (0.1)	210 (30)	16 (5)	1.4 (0.1)	0.2 (0.1)	–	–	Sand
SAM18-P24	Active	47	4	7.3 (0.2)	490 (270)	40 (6)	0.8 (0.1)	3.7 (1.4)	0.1 (0.1)	22.6 (1.6)	Sandy silt
	Permafrost	95	4	7.4 (0.2)	240 (80)	28 (7)	1.1 (0.2)	1.3 (1.0)	0.0 (0.1)	24.3 (0.0)	Silty sand
SAM18-P25	Active	53	5	7.6 (0.1)	470 (450)	31 (10)	1.0 (0.2)	3.1 (2.7)	0.2 (0.2)	18.5 (0.5)	Sand
	Permafrost	102	4	7.6 (0.2)	190 (20)	25 (5)	1.2 (0.1)	1.0 (0.7)	0.0 (0.1)	20.2 (0.0)	Sand

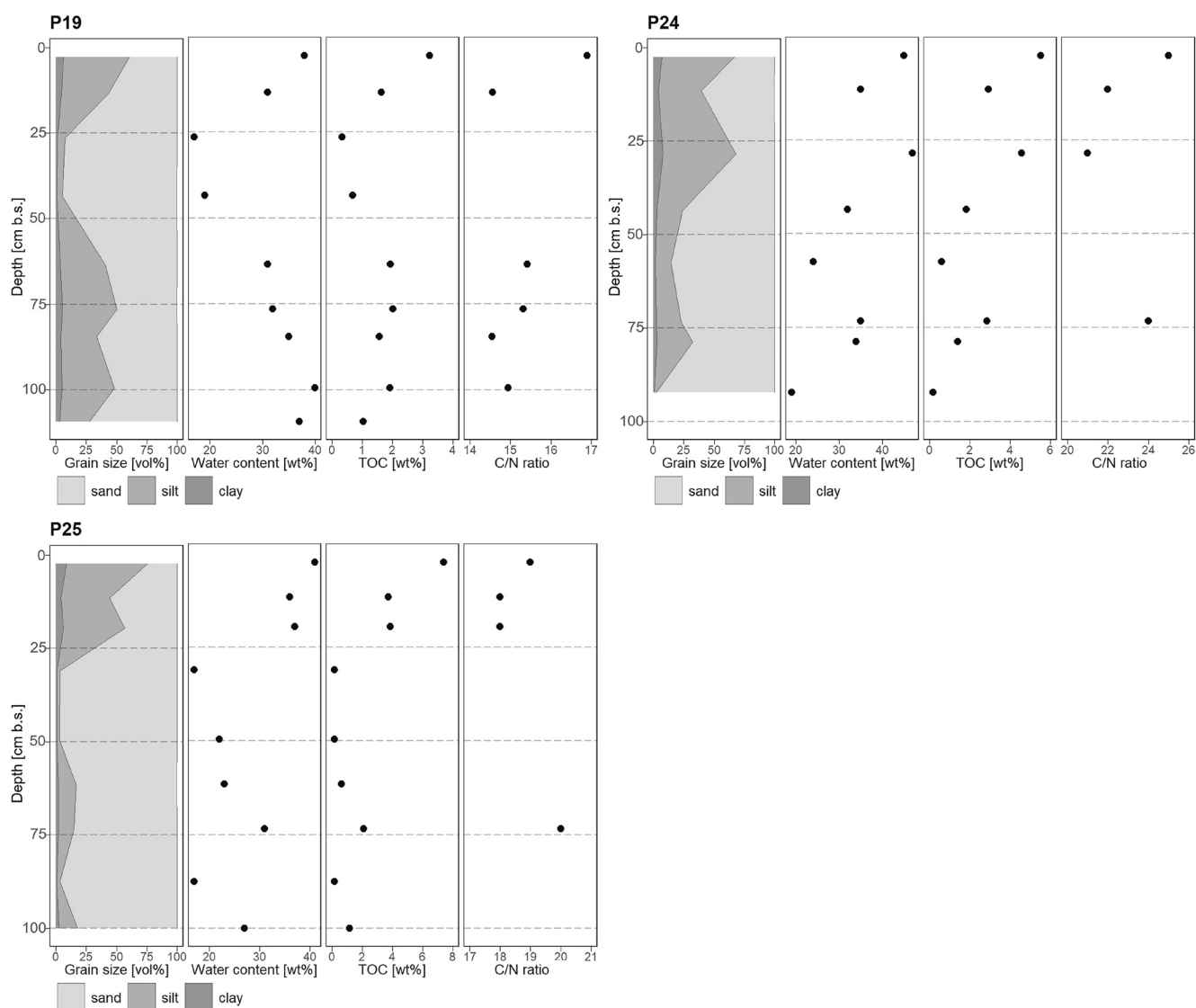


Figure 3. Sedimentology with depth for the three incubated cores, including grain size analysis, water content, total organic carbon content, and C/N ratios. (a) P19; (b) P24; (c) P25. The discrete depths analyzed are indicated by the points; grain size is interpolated between the points.

Table 3
Soil Organic Carbon and Soil Nitrogen Stocks for the Seven Soil Cores in the Reference Intervals of 0–30 cm Depths and 0–100 cm Depths

Core name	SOC stocks (kg C m ⁻²)		Soil N stocks (kg N m ⁻²)	
	0–30 cm	0–100 cm	0–30 cm	0–100 cm
KUR18-P18	2.35	4.50	0	0
KUR18-P19	4.91	15.25	0.30	0.85
SAM18-P20	3.37	14.37	0.09	0.72
SAM18-P21	6.67	19.45	0.32	1.07
SAM18-P22	0.26	3.10	0	0
SAM18-P24	8.98	18.56	0.40	0.61
SAM18-P25	9.83	15.01	0.53	0.68

non-vegetated sandbanks, the mean N stock of the vegetated active floodplains increased to 0.79 kg N m⁻² (0–100 cm).

Sediment ages were determined for selected layers of the cores P19, P24, and P25, which were incubated (Table S2 in Supporting Information S1). The ages in core P19 were all modern and included age inversions. For cores P24 and P25, the active layer samples were modern but the permafrost samples were older, reaching maximum ages of 1,590 ± 52 cal y BP. Accumulation rates were not calculated due to the age inversions and largely modern ages found in the sediment profiles (Table S2 in Supporting Information S1).

3.3. Incubations—Potential Carbon Release

3.3.1. Anaerobic Treatments

Over the course of the 356 day experiment under anaerobic conditions, the rates of maximum potential CH₄ production ranged from 0 to 7.3 μg CH₄-C

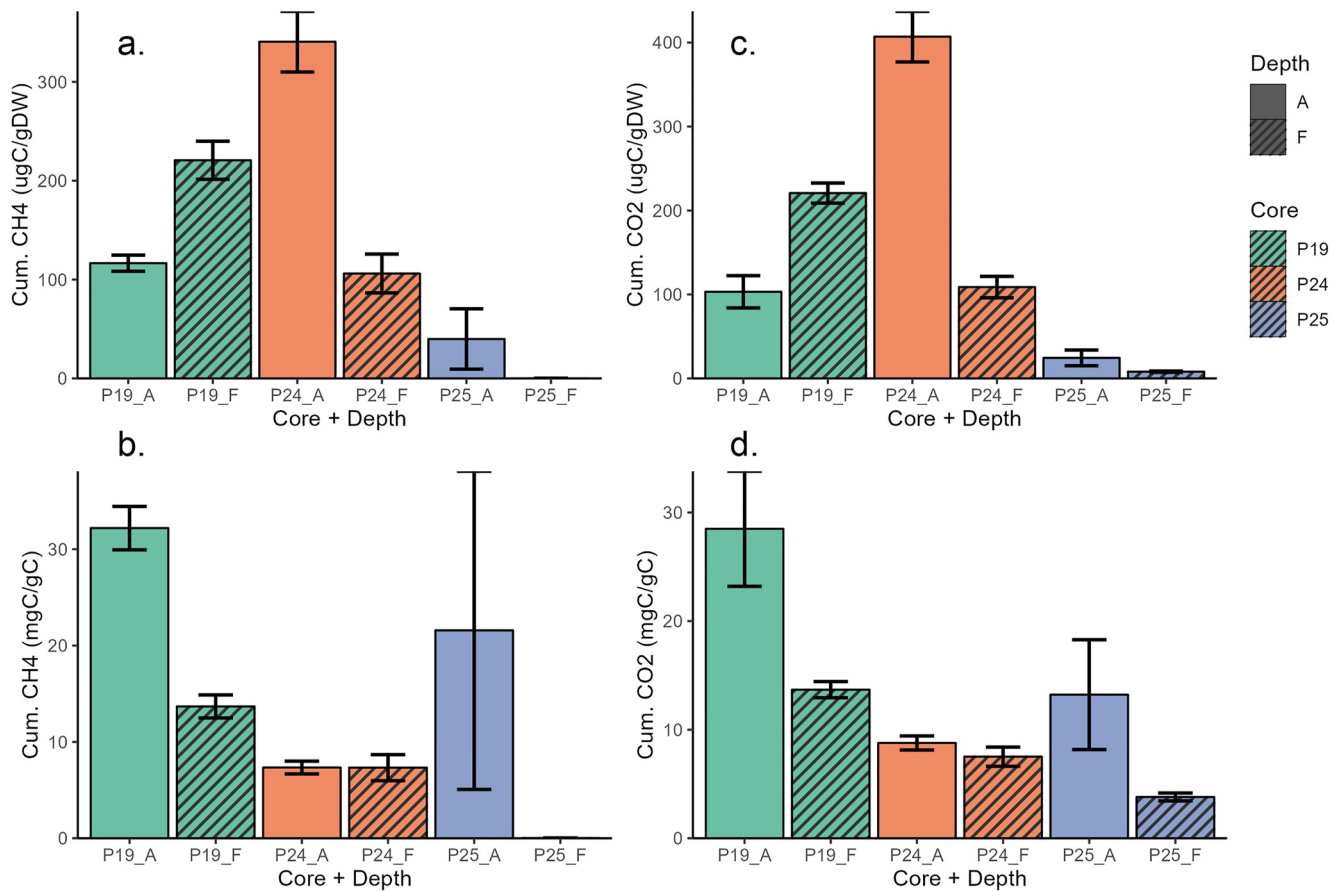


Figure 4. Anaerobic cumulative CH₄ (a and b: left panels) and CO₂ (c and d: right panels) production under anaerobic conditions for the six samples over the 356 day incubation period on a per gram dry weight basis (top panels) and normalized per gram carbon (bottom panels). The different cores are indicated by different colors; shading represents the permafrost (F/Frozen) layer, while unshaded values are indicative of the active layer (A) depths. Values and standard error are derived from the mean and standard deviations of the three laboratory replicates for each sample.

g DW⁻¹ d⁻¹ with a mean of $3.2 \pm 2.9 \mu\text{g CH}_4\text{-C g DW}^{-1} \text{d}^{-1}$ (Figure S3 in Supporting Information S1). When normalizing for the C content of the soils, maximum potential CH₄ production rates ranged from 1.0–710 $\mu\text{g CH}_4\text{-C g C}^{-1} \text{d}^{-1}$ across the samples, with a mean of $280 \pm 260 \mu\text{g CH}_4\text{-C g C}^{-1} \text{d}^{-1}$. Most peak potential CH₄ production rates occurred between days 45 and 80, although peak rates from samples P19-A and P25-F were strongly variable among the replicates (Figure S3 in Supporting Information S1). Peak CH₄ potential production rates in core P25-A were reached after a minimum of 152 days of incubation.

Cumulative CH₄ production from the three active floodplain cores (P19, P24, P25) ranged from 0 to 310 $\mu\text{g CH}_4\text{-C g DW}^{-1}$ under anaerobic conditions and less than 0.02 $\mu\text{g CH}_4\text{-C g DW}^{-1}$ under aerobic conditions over the 356 day experiment (Figure 4a). The pattern of CH₄ production differed between cores and depths (Figure 4a) with a significant depth by core interaction ($F_{2,11} = 81, p < 0.0001$). The active layer of P24 showed the highest cumulative CH₄ production ($340 \pm 30 \mu\text{g CH}_4\text{-C g DW}^{-1}$), followed by the permafrost layer of P19 ($221 \pm 19 \mu\text{g CH}_4\text{-C g DW}^{-1}$). P19-AL and P24-F released similar amounts (109–117 $\mu\text{g CH}_4\text{-C g DW}^{-1}$). Cumulative CH₄ production from P25 was the smallest; while CH₄ was produced by the active layer, the permafrost layer produced nearly negligible CH₄ during the course of the 356 day anaerobic incubation (Figure S3 in Supporting Information S1).

When normalized to the carbon content in the soils, cumulative CH₄ production differed both among the three cores ($F_{(2,11)} = 5.38, p = 0.02$) and with depth ($F_{(1,11)} = 14.0, p = 0.003$), although the core by depth interaction was not statistically significant ($F_{(2,11)} = 3.93, p = 0.05$). When comparing the three cores, anaerobic CH₄ production per gram of soil carbon were highest for P19 (Figure 4b), with a mean of $21 \pm 10 \text{ mg CH}_4\text{-C g C}^{-1}$ during the 356 day experiment, nearly or more than double the production in core P25 ($11 \pm 15 \text{ mg CH}_4\text{-C g C}^{-1}$) and

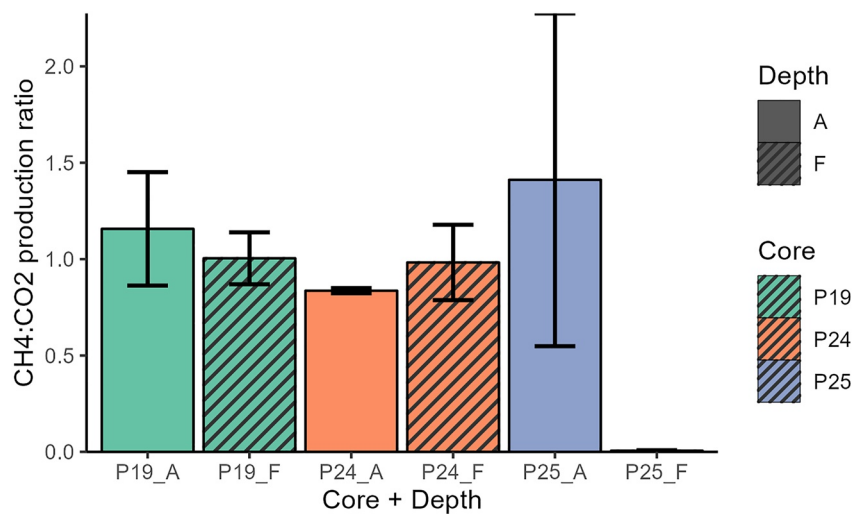


Figure 5. Ratio of CH₄:CO₂ production under anaerobic conditions for the six samples over the 356 day incubation period. The different cores are indicated by different colors; shading represents the permafrost (F/Frozen) layer, while unshaded values are indicative of the active layer (A) depths. Values and standard error are derived from the mean and standard deviations of the three laboratory replicates.

P24 (7.3 ± 0.9 mg CH₄-C g C⁻¹). Cumulative CH₄ production from the active layer was also more than double production in the permafrost layer (19 ± 14 and 7 ± 6 mg CH₄-C g C⁻¹, respectively).

Anaerobic rates of potential CO₂ production ranged from 0 to 13.1 μg CO₂-C g DW⁻¹ d⁻¹ across all the samples (Figure S3 in Supporting Information S1). When normalizing for the C content of the soils, potential anaerobic CO₂ production rates ranged from 0–37.5 μg CO₂-C gC⁻¹ d⁻¹ for all three analyzed cores and layers. Cumulative anaerobic CO₂ production ranged from 7 to 440 μg CO₂-C g DW⁻¹ and from 3.4 to 32.2 mg CO₂-C gC⁻¹ for all investigated cores and layers. The cumulative anaerobic CO₂ production differed both by depth and core (Figures 4c and 4d), with a significant depth by core interactions for both production per gram dry weight and per gram soil C (per gram DW: $F_{2,11} = 230$, $p < 0.0001$; per g C: $F_{2,11} = 8.4$, $p = 0.006$). Trends were similar to cumulative CH₄ production (Figure 4a), with highest anaerobic CO₂ production per gram dry weight occurring in core P24-A, which was nearly double the production in P19-F and ~300% larger than production in P19-A and P24-F. Anaerobic CO₂ production in core P25 was the smallest. When normalized to the soil C content, highest cumulative production occurred in P19-A (28 ± 5 mg CO₂-C gC⁻¹) and was nearly double the cumulative production from P19-F and P25-A (13 ± 5 mg CO₂-C gC⁻¹), followed by both depths from P24 and with smallest production coming from P25-F (3.8 ± 0.3 mg CO₂-C gC⁻¹; Figure 4d).

The ratio of cumulative CH₄:CO₂ produced in the anaerobic treatment differed both among cores and depths with a significant interaction (Figure 5; $F_{2,11} = 6.5$, $p = 0.01$). Cumulative CH₄:CO₂ ratios exceeded 1 in samples P25-A (1.4 ± 0.9) and P19-A (1.2 ± 0.3), and was near or slightly below 1 in the other samples except for P25-F, where it was less than 0.0 and significantly different from all other samples (Figure 5). Overall, CH₄ production comprised 0.5%–54% of total anaerobic C emissions. With the exclusion of P25-F, which differed significantly from all other samples, the mean across all cores and depths was $50 \pm 9\%$.

3.3.2. Aerobic Treatments

Rates of potential CO₂ production ranged from 0 to 23.3 μg CO₂-C g DW⁻¹ d⁻¹ across all the samples. When normalizing for the C content of the soils, potential CO₂ production rates ranged from 0 to 1.8 mg CO₂-C gC⁻¹ d⁻¹ for all three analyzed cores and layers. Across all samples, the highest potential CO₂ production rates occurred within the first week (mean = 4.7 days) except in one replicate. Rates of aerobic CO₂ production were relatively constant after incubation day 120 (Figure S4 in Supporting Information S1).

Cumulative CO₂ production after 356 days from the three active floodplain cores (P19, P24, P25) ranged from 25 to 1,640 μg CO₂-C g DW⁻¹ (mean = 570 ± 560 μg CO₂-C g DW⁻¹) under aerobic conditions over the 356 day experiment (Figure 6a). Cumulative CO₂ production per gram dry weight differed significantly among the cores

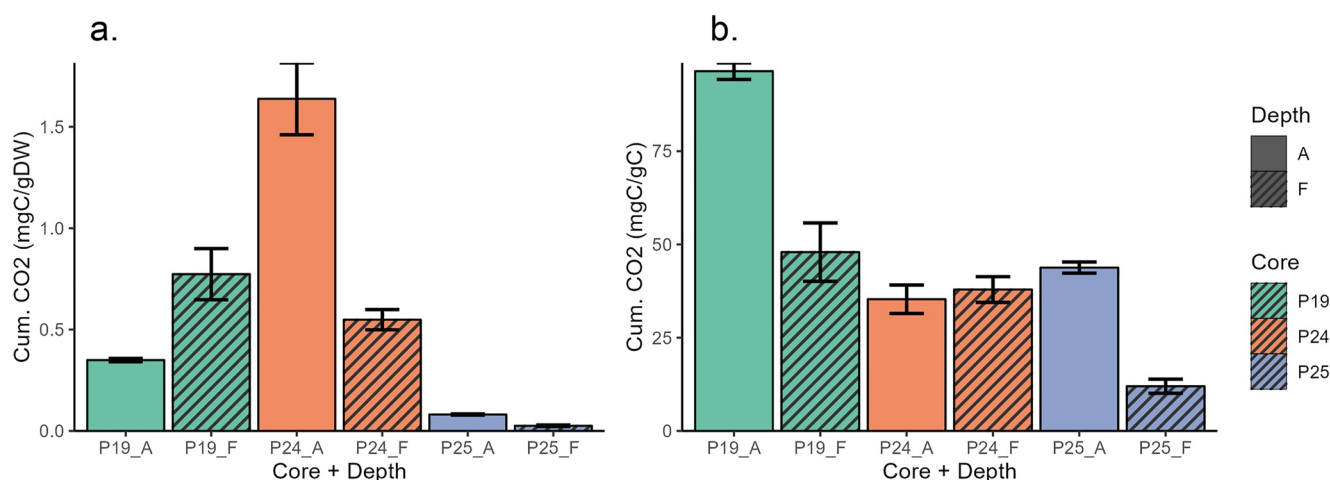


Figure 6. Cumulative CO₂ production under aerobic conditions for the six samples over the 356 day incubation period both: (a) per gram dry weight basis, and (b) normalized per gram carbon. The different cores are indicated by different colors; shading represents the permafrost (F/Frozen) layer, while unshaded values are indicative of the active layer (A) depths. Values and standard error are derived from the mean and standard deviations of the three laboratory replicates.

and depths with a significant core by depth interaction ($F_{(2,11)} = 108, p = 0.003$). Similar to anaerobic CO₂ production, aerobic CO₂ production from P24-A was significantly higher than the other cores ($1,640 \pm 180 \mu\text{g CO}_2\text{-C g DW}^{-1}$), and more than double the next highest sample P19-F ($773 \pm 130 \mu\text{g CO}_2\text{-C g DW}^{-1}$), and more than 60 times higher than the lowest sample, P25-F ($25 \pm 4 \mu\text{g CO}_2\text{-C g DW}^{-1}$). Cumulative aerobic CO₂ production was strongly correlated with soil C content ($F_{1,4} = 110, p < 0.001$), which also co-varied with silt content. When comparing the samples after normalizing for the C content, the cumulative CO₂ production per gram of soil carbon again showed similar trends to anaerobic CO₂ production with a significant core by depth interaction ($F_{(2,11)} = 62, p < 0.0001$). Cumulative production was highest for P19-A (Figure 6b), with a mean of $96 \pm 2 \text{ mg CO}_2\text{-C g C}^{-1}$ during the 356 day experiment, more than double the production in P19-F, the next highest ($47 \pm 8 \text{ mg CO}_2\text{-C g C}^{-1}$), which was similar to most other samples (35–43 \pm 4) except P25-F ($12 \pm 2 \text{ mg CO}_2\text{-C g C}^{-1}$). The cumulative C production per gram dry weight was strongly correlated with sample C content (Figure S5 in Supporting Information S1). After normalizing to the soil carbon content, there were no significant correlations to any tested soil properties.

Overall, the aerobic treatments emitted 60%–220% more carbon than the anaerobic treatments when considered C emitted as both CO₂ and CH₄ (Figure S6 in Supporting Information S1). Across all samples, the mean aerobic:anaerobic C production ratio was 2.3 ± 0.9 and did not significantly differ among depths ($F_{1,13} = 2.4, p = 0.15$) or cores ($F_{2,13} = 1.7, p = 0.23$). The ratio was highest in P25-F, where the aerobic:anaerobic C production ratio was greater than 3. It was similar among the other samples, ranging from 1.5 to 2 for cores P19 at both depths and sample P25-A, although this sample was highly variable.

4. Discussion

4.1. C Stocks and Processes in Active Floodplains

These cores from active floodplain soils in the Lena River Delta showed that overall the soils are exceptionally sandy, indicating the importance of fluvial and depositional processes in this environment. Overall, the average sand fraction of all cores was high (Table 2, Figure 2); the main component of the soil texture in all incubated samples was sand. However, the grain size distribution of the analyzed samples indicated a high heterogeneity in the soils of the active floodplains. The sand, silt and clay fractions had a wide range (sand: 24.5%–99.4%, silt: 0.5%–66.9%, clay: 0%–8.6%) and distribution varied from unimodal to polymodal and from very poorly sorted to well sorted (Figure 2). Fluvial origin and continuous episodic reworking result in floodplain soils that are composed of stratified medium to fine sands and silts as well as layers of organic matter and peat (Boike et al., 2013). A peak in the sand fraction indicates that flowing water is the dominant transport process, whereas lower stream flow may lead to deposition of coarser silt. The mixture of unimodal, bimodal, trimodal, and polymodal distribution curves also indicates that the sediments may have been deposited not only by river,

but also by alluvial and lacustrine processes (Fuchs et al., 2018b). Overall, the mixed grain size signal reflects that the active floodplains are located in a very dynamic landscape, characterized by migrating river channels, spring flooding, and various depositional processes. The influence of periodic or spring flooding is also supported by the relative enhancement in conductivity observed in active layers of several cores ($>400 \mu\text{S cm}^{-1}$; Table 2), which agrees well with surface river water conductivity in the center of the Olenekskaya Channel ($99\text{--}490 \mu\text{S cm}^{-1}$), the creek between Samoylov and Kurungnakh Island, which is responsible for early season flooding of the investigated active floodplains (Juhls et al., 2020).

The high heterogeneity of C content with depth and age-inversions in the ^{14}C profile might indicate the importance of depositional processes rather than soil-forming processes (Fuchs et al., 2018b). Overall, TOC varied by a factor of 70 between cores and with depth ($<0.1\text{--}7.4\%$; Table 2), indicating that active floodplain soils are very heterogeneous not only among the cores but also with depth. The surface soil sample often had the highest carbon concentrations (Figure 3), which may be attributed to the presence of fresh organic matter due to vegetation (Knoblauch et al., 2013). However, some cores (P19, P24) also showed deeper organic-rich layers indicating a burial of sediments either through cryoturbation or by periodic deposition of a sandy layer on top of the existing vegetation during spring flooding (Figure 3; Figure S1 in Supporting Information S1). Sediment burial associated with deltaic and fluvial processes is also supported by the sedimentology showing the dominance of depositional processes (Figure 2), which can be expected in these low lying floodplain environments. However, the buried C layers and deep-distributed C stocks, with the majority falling beneath 30 cm (Table 3) is not visible from the surface vegetation, making vegetation-based soil mapping challenging in these environments (Palmtag et al., 2022).

The cores that were dated from this region in the Lena River Delta using radiocarbon relatively young material deposited in the first meter of soil. The radiocarbon ages in this study ranged from modern to $1,590 \pm 52.3$ years BP (Table S2 in Supporting Information S1). In cores P24 and P25, a increase of age with depth could be recognized, whereas two age inversions occurred in core P19 (Table S2 in Supporting Information S1). It is unclear whether sediment re-working is responsible for these age inversions, given also the increase in TOC with depth, or whether the age inversions were somehow contaminated either during field sampling or by choosing material inappropriate for ^{14}C dating. In general, it is difficult to date organic material in a delta setting, as sediment and organic matter can originate further upstream or get reworked (Stanley, 2001). However, age inversions are common and problematic in other lowlying permafrost landscapes and other floodplains. This also has been documented in river-adjacent permafrost peatlands in Alaska (Nichols et al., 2017). Therefore, calculation of apparent sediment and C accumulation rates was not undertaken here and must be treated with some caution.

This study indicates the importance of active floodplains as C and N permafrost deposits, although limited field data are available from active floodplains across the Arctic. Active floodplains are areas not only of soil-forming processes but also deltaic depositional processes, which incorporate C and N deep into active floodplain sediments (Figure 3). While the soils in the active floodplains (e.g., Fuchs et al., 2018b; Zubrzycki et al., 2013) generally have a lower C density than soils in other tundra environments (e.g., Hugelius et al., 2010; Palmtag et al., 2022) due to the larger fraction of sandy deposits and sand-dominated texture in soil layers, they cover a relatively large area ($8,830 \text{ km}^2$, 40% of land area) within the Lena River Delta Region and also contain significant buried C stocks from depositional processes (Zubrzycki et al., 2013). This indicates that active floodplains should not be underestimated when determining C and N permafrost deposits, particularly in regions with large deltas. For further robust and representative estimates, the strong spatial variability of active floodplain soils (both the inhomogeneous distribution of study sites and varying C and N contents within soil depth) must be considered in future data collection (Zubrzycki et al., 2013).

4.2. Decomposability and Potential C Production of Active Floodplains

The cumulative potential C production after 356 days showed similar patterns across cores and depths in both aerobic and anaerobic treatments for both CH_4 and CO_2 production (Figures 4 and 6). Across the selected cores, the highest cumulative production of CO_2 and CH_4 occurred in the active layer of core P24 (P24-A) and the lowest cumulative production occurred in core P25, with very small production from the P25 permafrost sample (P25-F). The cumulative C production per gram dry weight was strongly correlated with sample C content (Figure S5 in Supporting Information S1). After normalizing for the differences in C content across the sample, there were no significant predictors of cumulative potential C production, including sand, silt and clay fraction, C/N ratio

or radiocarbon age. Additionally, nearly all the statistical analyses showed significant core by depth interactions, with the exception of CH₄ production per g C. This indicates that the depth effect (active layer vs. permafrost) was generally not consistent across the cores; the cumulative C production could not be predicted from either the core or the depth. This highlights the challenge of these active floodplain samples: not only are they strongly variable among sampling locations, but they also vary strongly with depth for both potential C production (Figures 4 and 6) and for other characteristics (Figures 2 and 3). Furthermore, these below-ground characteristics are difficult to predict based on the surface vegetation, which is similar among the cores sampled intensively (P19, P24, P25 in Table 1).

The null hypothesis in this study was that the C production would differ between permafrost and active layer samples because of C inputs from surface vegetation and decompositional processes that occur in the active layer. Some earlier studies showed that active layer soils produced more C in incubation experiments than permafrost soils (Lee et al., 2012; Treat et al., 2014, 2015). Here, samples from the active layer produced significantly more CH₄ when normalized per gram soil C (Figure 4b) than permafrost samples and could be due to fresher substrate from plant inputs. In these active floodplain sites, there was no consistent difference in C produced between active layer and permafrost samples for most other analyses (Figures 4 and 6). This is demonstrated by the difference in cumulative CO₂ production under aerobic conditions between P24-F replicates and P25-F replicates: both samples were from similar aged material (from ~1,590 cal y BP, Table S2 in Supporting Information S1) and similar depths. In sample P19-A, 10 ± 2% of the initial carbon was lost from permafrost after the ~1 year incubation, which was similar to active layer and permafrost samples of other cores (Figures 4 and 6). However, only 1% of the initial C was lost from permafrost of core P25 under “ideal” conditions for microbial decomposition. In these floodplain sites, it is likely that the decomposability of the organic material in the permafrost is also dependent on the same dynamic depositional processes that occur in floodplains; sediments buried during flooding determine the physical soil properties (e.g., buried soil horizons) and decomposability of these deeper sediments, which again makes generalization within the active floodplain soils difficult.

Comparing cumulative C losses in these active floodplain soils from an Arctic delta across other permafrost soils shows interesting trends. In this study, these soils lost on average 4.6 ± 2.8% of their initial C content after approximately 1 year of incubation at 20°C under aerobic conditions (Figure 6b) and 2.6 ± 2.0% under anaerobic conditions (Figures 4b and 4d). In an earlier synthesis of long-term aerobic incubations of permafrost region soils, Schädel et al. (2014) showed that mineral soils generally lost less than 5% and organic soils lost 6% of their initial soil carbon after 1 year, but at a much lower reference temperature (5 vs. 20°C in this study, both aerobic conditions). This indicates that the organic matter at this site is not exceptionally fast-cycling or biologically available under warm, aerobic conditions. Water contents in the incubated samples were low (25%–40%), but even these low water contents have been shown to have similar C production to samples with higher water content, for example, moisture was not limiting (Wickland & Neff, 2008).

Anaerobic C production and the contribution of CH₄ to total anaerobic C production are exceptionally high in these samples from the active floodplain, despite being generally sandy. In this study, the aerobic:anaerobic C production ratio ranged from 1.6 to 3.2 with a mean of 2.3 ± 0.9 (Figure S6 in Supporting Information S1) but showed no significant differences between active layer and permafrost samples. The aerobic:anaerobic production ratio in this study was consistently lower by 20%–50% than in an earlier synthesis by Schädel et al. (2016) of permafrost soil incubations, where the production ratio differed between active layer (median ratio: 3.3) and permafrost (median ratio: 4.2) soils. Given that aerobic C cycling is average to low in these soils, this indicates that anaerobic cycling is very active. In the anaerobic treatment, cumulative CH₄ production accounted for 50 ± 9% of total anaerobic C production (Figure 5). This is significantly higher than reported 30%–40% of anaerobic C production for tundra, boreal forests, and peatlands in the permafrost region at a comparable ~20°C incubation temperature (Schädel et al., 2016).

Several mechanisms could result in strong anaerobic C mineralization and CH₄ production in these soils, such as the availability of alternative electron acceptors, microbial community composition, the origins of the C substrate mineralized, or some combination of these factors. The relatively high rates may result from the periodic inundation associated with active floodplains and indicated in situ by the observations of redox features in some of the soil profiles (Figure S1 in Supporting Information S1); on the other hand, in sample P25-F both redox features and low CH₄ production were observed. An earlier study using floodplain mineral soils on Samoylov Island found relatively similar methanogenic communities across the depths within a soil profile (Ganzert

et al., 2007), which they attributed to the regular flooding. Why periodic flooding enhances the potential CH_4 production rates is unclear; earlier comparisons have shown highest anaerobic C production in incubations from permafrost soils with fluctuating water tables (Treat et al., 2015). In temperate soils, lab experiments simulating flooding via rising groundwater levels showed significantly higher CH_4 production rates than the addition of rainwater; this was attributed to the activation of methanogens at depth in the core (Smith et al., 2017). Periodic flooding may replenish nutrient supplies and enhance vegetation productivity, resulting in root exudates to fuel methanogenesis (Bastviken et al., 2023) and was hypothesized to be critical for the observation of high CH_4 fluxes from Arctic floodplain soils along with vegetative CH_4 transport (van Huissteden et al., 2005). In this *ex-situ* study, plant transport is not a factor, but the role of plant root exudates or recent flood deposits could be indicated from the higher CH_4 production per gram soil C in the active layer than the permafrost (Figure 4b). All together, these results indicate that multiple processes contribute to the active anaerobic C cycling in periodically flooded systems. Understanding the interactions between flooding dynamics, mineralogy (e.g., iron oxidation), methanogens and other anaerobic-tolerant microbes, and plant dynamics should be further investigated to better understand potential hotspots for CH_4 emissions in Arctic landscapes.

Methane production rates in these mineral soil samples were also higher than in many other types of soils and sites. The mean maximum CH_4 production rates across all samples in this study were $280 \pm 260 \mu\text{g C gC}^{-1} \text{d}^{-1}$, which were more than 80 times higher than the maximum CH_4 production rates for all mineral soils ($3.3 \pm 0.5 \mu\text{g C gC}^{-1} \text{d}^{-1}$) and more than 10 times higher than organic soils ($18.7 \pm 12.1 \mu\text{g C gC}^{-1} \text{d}^{-1}$) in an earlier synthesis of anaerobic incubations from permafrost region soils (Treat et al., 2015). This very large difference appears to be driven by the low carbon contents in these sandy floodplain soils; when maximum rates of CH_4 production per gram dry weight are compared between the two incubation studies, the maximum rates in this study ($3.2 \pm 3.0 \mu\text{g C g DW}^{-1} \text{d}^{-1}$) are still 15x larger than rates reported for mineral soils ($0.2 \pm 0.0 \mu\text{g C gDW}^{-1} \text{d}^{-1}$) but about 30% lower than rates in organic soils ($4.5 \pm 0.7 \mu\text{g C gDW}^{-1} \text{d}^{-1}$). The rates reported by Treat et al. (2015) were not normalized for incubation temperature and could result in relatively low production rates relative to this study because these samples were incubated at 20°C , a temperature unlikely to be found for extended periods in field conditions. Still, this is unlikely to explain orders of magnitude differences between the findings for mineral soils and indicate high efficiency of CH_4 production in these samples. This is similarly indicated by the $\text{CH}_4:\text{CO}_2$ production ratio (Figure 5). The high ratios indicate that the methanogenic community is viable and active in these active floodplain soils as shown in this study and in an earlier analysis at a nearby lowland site (Laurent et al., 2023); high CH_4 fluxes have been observed in situ from other floodplains in Siberia (Terentieva et al., 2019; van Huissteden et al., 2005). Field observations from other tundra sites in this region show similar trends: CH_4 emissions are driven by production in deep soils which occurs when they are warm enough and redox conditions are favorable, bringing the $\text{CH}_4:\text{CO}_2$ production ratio closer to 1:1 later in the growing and thaw season (Galera et al., 2023). Additional field observations of CH_4 and CO_2 fluxes during the growing season would help to illustrate whether the anaerobic production potentials demonstrated by this incubation translate into significant CH_4 and CO_2 fluxes measured in the field.

5. Conclusions

The active floodplain soils from the Lena River Delta in Siberia showed exceptionally high variability both among the coring locations and with depth in terms of C stocks and potential C production. The spatial variability affected both the physical soil properties and the potential C mineralization in incubations. These spatial heterogeneity effects resulted in few differences between potential C production in permafrost and active layers. The below-ground properties did not correspond with the above-ground vegetation, which was similar across many of the coring locations for both the incubated and the other cores. This makes the below-ground properties nearly impossible to predict based on the surface vegetation or surface soil properties. Instead, below-ground C stocks and sediment properties are most likely related to the depositional and erosional processes that re-work sediment in active floodplain areas like we sampled in the Lena River Delta.

However, when we compare these active floodplain sites to other Arctic sites, their significance becomes clearer. While C densities in the top 1 m of these active floodplains are generally low due to the prevalence of sand in the profile, thick sediments, buried C-rich layers and high sediment accumulation rates make these active floodplain deposits an important consideration in regional C stock estimates. The rates of C production from these soils indicate moderate C quality relative to other permafrost sites under aerobic conditions, but potential anaerobic CH_4

and CO₂ production was exceptionally high both relative to aerobic production in these sites and when compared across sites. However, limited field measurements are available to assess C balance in these active floodplain systems. Future measurements in other locations with additional measurements of microbial communities, soil chemistry, and mineralogy would help to determine how these floodplains function in regards to biogeochemical cycles, which is important to understand in regions like the Lena River Delta, where these floodplains cover significant areas.

Data Availability Statement

The soil properties, sedimentology, and potential CO₂ and CH₄ production data used for the analysis of active floodplains in the Lena River Delta in this study are available at Pangaea.de via <https://doi.pangaea.de/10.1594/PANGAEA.959669> with CCBY-4.0 license (Treat et al., 2023).

Acknowledgments

We thank A. Runge for help with soil sampling, O. Burckhardt, M. Laurent, J. Vollmer, and L. Golde for help with incubation sampling and analysis. We acknowledge funding from European Research Council (ERC) Horizon 2020 Research and Innovation (Grant Agreement no. 851181), the German Ministry for Education and Research (KoPF, CarboPerm), and the Helmholtz Innovation and Networking Fund. This work resulted from a MS thesis in the Department of Environmental Sciences at Albert-Ludwigs-University, Freiburg, Germany; we acknowledge the thesis supervision of C. Werner and G. Grosse. Open Access funding enabled and organized by Projekt DEAL.

References

- Bastviken, D., Treat, C. C., Pangala, S. R., Gauci, V., Enrich-Prast, A., Karlson, M., et al. (2023). The importance of plants for methane emission at the ecosystem scale. *Aquatic Botany*, *184*, 103596. <https://doi.org/10.1016/j.aquabot.2022.103596>
- Biskaborn, B. K., Smith, S. L., Noetzi, J., Matthes, H., Vieira, G., Streletskiy, D. A., et al. (2019). Permafrost is warming at a global scale. *Nature Communications*, *10*(1), 264. <https://doi.org/10.1038/s41467-018-08240-4>
- Blott, S. J., & Pye, K. (2001). GRADISTAT: A grain size distribution and statistics package for the analysis of unconsolidated sediments. *Earth Surface Processes and Landforms*, *26*(11), 1237–1248. <https://doi.org/10.1002/esp.261>
- Boike, J., Kattenstroth, B., Abramova, K., Bornemann, N., Chetverova, A., Fedorova, I., et al. (2013). Baseline characteristics of climate, permafrost and land cover from a new permafrost observatory in the Lena River Delta, Siberia (1998–2011). *Biogeosciences*, *10*(3), 2105–2128. <https://doi.org/10.5194/bg-10-2105-2013>
- Boike, J., Nitzbon, J., Anders, K., Grigoriev, M., Bolshiyarov, D., Langer, M., et al. (2019). A 16-year record (2002–2017) of permafrost, active-layer, and meteorological conditions at the Samoylov Island Arctic permafrost research site, Lena River delta, northern Siberia: An opportunity to validate remote-sensing data and land surface, snow, and permafrost models. *Earth System Science Data*, *11*(1), 261–299. <https://doi.org/10.5194/essd-11-261-2019>
- French, H., & Shur, Y. (2010). The principles of cryostratigraphy. *Earth-Science Reviews*, *101*(3), 190–206. <https://doi.org/10.1016/j.earscirev.2010.04.002>
- Fuchs, M., Grosse, G., Jones, B. M., Strauss, J., Baughman, C. A., & Walker, D. (2018a). Measured water content, carbon and nitrogen data from permafrost cores of the Ikpikuk River and Fish Creek River delta [Dataset]. Pangaea.de. <https://doi.org/10.1594/PANGAEA.895541>
- Fuchs, M., Grosse, G., Jones, B. M., Strauss, J., Baughman, C. A., & Walker, D. A. (2018b). Sedimentary and geochemical characteristics of two small permafrost-dominated Arctic river deltas in northern Alaska. *arktos*, *4*(1), 1–18. <https://doi.org/10.1007/s41063-018-0056-9>
- Fuchs, M., Lenz, J., Jock, S., Nitze, I., Jones, B. M., Strauss, J., et al. (2018). Basic sediment characteristics of permafrost cores in the Teshekpuk Lake Area on the Arctic Coastal Plain, Northern Alaska [Dataset]. Pangaea.de. <https://doi.org/10.1594/PANGAEA.895163>
- Galera, L. D. A., Eckhardt, T., Beer, C., Pfeiffer, E.-M., & Knoblauch, C. (2023). Ratio of in situ CO₂ to CH₄ production and its environmental controls in polygonal tundra soils of Samoylov Island, Northeastern Siberia. *Journal of Geophysical Research: Biogeosciences*, *128*(4), e2022JG006956. <https://doi.org/10.1029/2022JG006956>
- Ganzert, L., Jurgens, G., Münster, U., & Wagner, D. (2007). Methanogenic communities in permafrost-affected soils of the Laptev Sea coast, Siberian Arctic, characterized by 16S rRNA gene fingerprints. *FEMS Microbiology Ecology*, *59*(2), 476–488. <https://doi.org/10.1111/j.1574-6941.2006.00205.x>
- Harden, J. W., Koven, C. D., Ping, C.-L., Hugelius, G., McGuire, A. D., Camill, P., et al. (2012). Field information links permafrost carbon to physical vulnerabilities of thawing. *Geophysical Research Letters*, *39*(15), L15704. <https://doi.org/10.1029/2012gl015958>
- Harden, J. W., Sundquist, E. T., Stallard, R. F., & Mark, R. K. (1992). Dynamics of soil carbon during deglaciation of the Laurentide ice-sheet. *Science*, *258*(5090), 1921–1924. <https://doi.org/10.1126/science.258.5090.1921>
- Harris, S. A., French, H. M., Heginbottom, J. A., Johnston, G. H., Ladanyi, B., Segó, D. C., & van Everdingen, R. O. (1988). *Glossary of permafrost and related ground-ice terms* (157 pp.). Associate Committee on Geotechnical Research, National Research Council of Canada. Retrieved from https://globalcryospherewatch.org/reference/glossary_docs/permafrost_and_ground_terms_canada.pdf
- Hugelius, G., Bockheim, J. G., Camill, P., Elberling, B., Grosse, G., Harden, J. W., et al. (2013). A new data set for estimating organic carbon storage to 3 m depth in soils of the northern circumpolar permafrost region. *Earth System Science Data*, *5*(2), 393–402. <https://doi.org/10.5194/essd-5-393-2013>
- Hugelius, G., Kuhry, P., Tarnocai, C., & Virtanen, T. (2010). Soil organic carbon pools in a periglacial landscape: A case study from the central Canadian Arctic. *Permafrost and Periglacial Processes*, *21*(1), 16–29. <https://doi.org/10.1002/ppp.677>
- Hugelius, G., Strauss, J., Zubrzycki, S., Harden, J. W., Schuur, E. A. G., Ping, C. L., et al. (2014). Estimated stocks of circumpolar permafrost carbon with quantified uncertainty ranges and identified data gaps. *Biogeosciences*, *11*(23), 6573–6593. <https://doi.org/10.5194/bg-11-6573-2014>
- Juhs, B., Stedmon, C. A., Morgenstern, A., Meyer, H., Holeyman, J., Heim, B., et al. (2020). Identifying drivers of seasonality in Lena River biogeochemistry and dissolved organic matter fluxes. *Frontiers in Environmental Science*, *8*, 15. <https://doi.org/10.3389/fenvs.2020.00053>
- Knoblauch, C., Beer, C., Sosnin, A., Wagner, D., & Pfeiffer, E.-M. (2013). Predicting long-term carbon mineralization and trace gas production from thawing permafrost of Northeast Siberia. *Global Change Biology*, *19*(4), 1160–1172. <https://doi.org/10.1111/gcb.12116>
- Köchy, M., Hiederer, R., & Freibauer, A. (2015). Global distribution of soil organic carbon – Part 1: Masses and frequency distributions of SOC stocks for the tropics, permafrost regions, wetlands, and the world. *Soil*, *1*(1), 351–365. <https://doi.org/10.5194/soil-1-351-2015>
- Kruse, S., Bolshiyarov, D., Grigoriev, M. N., Morgenstern, A., Pstryakova, L., Tsbizov, L., & Udke, A. (2019). *Russian-German Cooperation: Expeditions to Siberia in 2018* (Vol. 734). Alfred Wegener Institute for Polar and Marine Research.
- Laurent, M., Fuchs, M., Herbst, T., Runge, A., Liebner, S., & Treat, C. (2023). Relationships between greenhouse gas production and landscape position during short-term permafrost thaw under anaerobic conditions in the Lena Delta. *Biogeosciences*, *2022*(11), 2049–2064. <https://doi.org/10.5194/bg-20-2049-2023>

- Lee, H., Schuur, E. A. G., Inglett, K. S., Lavoie, M., & Chanton, J. P. (2012). The rate of permafrost carbon release under aerobic and anaerobic conditions and its potential effects on climate. *Global Change Biology*, *18*(2), 515–527. <https://doi.org/10.1111/j.1365-2486.2011.02519.x>
- Michaelson, G. J., Ping, C. L., & Kimble, J. M. (1996). Carbon storage and distribution in tundra soils of Arctic Alaska, USA. *Arctic and Alpine Research*, *28*(4), 414–424. <https://doi.org/10.2307/1551852>
- Mollenhauer, G., Grotheer, H., Gentz, T., Bonk, E., & Hefter, J. (2021). Standard operation procedures and performance of the MICADAS radiocarbon laboratory at Alfred Wegener Institute (AWI), Germany. *Nuclear Instruments and Methods in Physics Research Section B: Beam Interactions with Materials and Atoms*, *496*, 45–51. <https://doi.org/10.1016/j.nimb.2021.03.016>
- Nichols, J. E., Peteet, D. M., Frolking, S., & Karavias, J. (2017). A probabilistic method of assessing carbon accumulation rate at Innvait Creek Peatland, Arctic Long Term Ecological Research Station, Alaska. *Journal of Quaternary Science*, *32*(5), 579–586. <https://doi.org/10.1002/jqs.2952>
- Obu, J., Westermann, S., Bartsch, A., Berdnikov, N., Christiansen, H. H., Dashtseren, A., et al. (2019). Northern Hemisphere permafrost map based on TTOP modelling for 2000–2016 at 1 km² scale. *Earth-Science Reviews*, *193*, 299–316. <https://doi.org/10.1016/j.earscirev.2019.04.023>
- Overeem, I., Nienhuis, J. H., & Piliouras, A. (2022). Ice-dominated Arctic deltas. *Nature Reviews Earth & Environment*, *3*(4), 225–240. <https://doi.org/10.1038/s43017-022-00268-x>
- Palmtag, J., Obu, J., Kuhry, P., Richter, A., Siewert, M. B., Weiss, N., et al. (2022). A high spatial resolution soil carbon and nitrogen dataset for the northern permafrost region based on circumpolar land cover upscaling. *Earth System Science Data*, *14*(9), 4095–4110. <https://doi.org/10.5194/essd-14-4095-2022>
- Ping, C. L., Michaelson, G. J., Guo, L. D., Jorgenson, M. T., Kanevskiy, M., Shur, Y., et al. (2011). Soil carbon and material fluxes across the eroding Alaska Beaufort Sea coastline. *Journal of Geophysical Research*, *116*(G2), 12. <https://doi.org/10.1029/2010jg001588>
- Rantanen, M., Karpechko, A. Y., Lipponen, A., Nordling, K., Hyvärinen, O., Ruosteenoja, K., et al. (2022). The Arctic has warmed nearly four times faster than the globe since 1979. *Communications Earth & Environment*, *3*(1), 168. <https://doi.org/10.1038/s43247-022-00498-3>
- R Development Core Team. (2008). *R: A language and environment for statistical computing*. R Foundation for Statistical Computing. Retrieved from <http://www.R-project.org>
- Reimer, P. J., Austin, W. E. N., Bard, E., Bayliss, A., Blackwell, P. G., Bronk Ramsey, C., et al. (2020). The IntCal20 Northern Hemisphere radiocarbon age calibration curve (0–55 cal kBP). *Radiocarbon*, *62*(4), 725–757. <https://doi.org/10.1017/RDC.2020.41>
- Robertson, G. P., Wedin, D., Groffman, P. M., Blair, J. M., Holland, E. A., Nadelhoffer, K. J., & Harris, D. (1999). Soil carbon and nitrogen availability: Nitrogen mineralization, nitrification, and soil respiration potentials. In G. P. Robertson, D. C. Coleman, C. S. Bledsoe, & P. Sollins (Eds.), *Standard Soil Methods for Long-Term Ecological Research* (pp. 258–271). Oxford University Press.
- Schädel, C., Bader, M. K. F., Schuur, E. A. G., Biasi, C., Bracho, R., Capek, P., et al. (2016). Potential carbon emissions dominated by carbon dioxide from thawed permafrost soils. *Nature Climate Change*, *6*(10), 950–953. <https://doi.org/10.1038/nclimate3054>
- Schädel, C., Schuur, E. A. G., Bracho, R., Elberling, B., Knoblauch, C., Lee, H., et al. (2014). Circumpolar assessment of permafrost C quality and its vulnerability over time using long-term incubation data. *Global Change Biology*, *20*(2), 641–652. <https://doi.org/10.1111/gcb.12417>
- Schirrmeister, L., Oezen, D., & Geyh, M. A. (2002). ²³⁰Th/U dating of frozen peat, Bol'shoy Lyakhovskiy Island (Northern Siberia). *Quaternary Research*, *57*(2), 253–258. <https://doi.org/10.1006/qres.2001.2306>
- Schuur, E. A. G., McGuire, A. D., Schädel, C., Grosse, G., Harden, J. W., Hayes, D. J., et al. (2015). Climate change and the permafrost carbon feedback. *Nature*, *520*(7546), 171–179. <https://doi.org/10.1038/nature14338>
- Schwamborn, G., Rachold, V., & Grigoriev, M. N. (2002). Late Quaternary sedimentation history of the Lena Delta. *Quaternary International*, *89*(1), 119–134. [https://doi.org/10.1016/s1040-6182\(01\)00084-2](https://doi.org/10.1016/s1040-6182(01)00084-2)
- Siewert, M. B., Hugelius, G., Heim, B., & Faucherre, S. (2016). Landscape controls and vertical variability of soil organic carbon storage in permafrost-affected soils of the Lena River Delta. *Catena*, *147*, 725–741. <https://doi.org/10.1016/j.catena.2016.07.048>
- Smith, A. P., Bond-Lamberty, B., Benscoter, B. W., Tfaily, M. M., Hinkle, C. R., Liu, C., & Bailey, V. L. (2017). Shifts in pore connectivity from precipitation versus groundwater rewetting increases soil carbon loss after drought. *Nature Communications*, *8*(1), 1335. <https://doi.org/10.1038/s41467-017-01320-x>
- Stanley, J.-D. (2001). Dating modern deltas: Progress, problems, and prognostics. *Annual Review of Earth and Planetary Sciences*, *29*(1), 257–294. <https://doi.org/10.1146/annurev.earth.29.1.257>
- Terentieva, I. E., Sabrekov, A. F., Ilyasov, D., Ebrahimi, A., Glagolev, M. V., & Maksyutov, S. (2019). Highly dynamic methane emission from the West Siberian boreal floodplains. *Wetlands*, *39*(2), 217–226. <https://doi.org/10.1007/s13157-018-1088-4>
- Treat, C. C., Fuchs, M., Herbst, T., Laurent, M., Liebner, S., & Vetier, A. (2023). Below-ground carbon stocks, soil properties, and potential CO₂ and CH₄ production in the central Lena River Delta, Kurungnakh and Samoylov Islands from 12 permafrost profiles sampled in 2018 [Dataset]. Pangaea.de. <https://doi.pangaea.de/10.1594/PANGAEA.959669>
- Treat, C. C., Natali, S. M., Ernakovich, J., Iversen, C. M., Lupascu, M., McGuire, A. D., et al. (2015). A pan-Arctic synthesis of CH₄ and CO₂ production from anoxic soil incubations. *Global Change Biology*, *21*(7), 2787–2803. <https://doi.org/10.1111/gcb.12875>
- Treat, C. C., Wollheim, W. M., Varner, R. K., Grandy, A. S., Talbot, J., & Frolking, S. (2014). Temperature and peat type control CO₂ and CH₄ production in Alaskan permafrost peats. *Global Change Biology*, *20*(8), 2674–2686. <https://doi.org/10.1111/gcb.12572>
- van Huissteden, J., Maximov, T. C., & Dolman, A. J. (2005). High methane flux from an arctic floodplain (Indigirka lowlands, eastern Siberia). *Journal of Geophysical Research*, *110*(G2), G02002. <https://doi.org/10.1029/2005JG000010>
- Walker, H. J. (1998). Arctic deltas. *Journal of Coastal Research*, *14*(3), 718–738.
- Wickland, K. P., & Neff, J. C. (2008). Decomposition of soil organic matter from boreal black spruce forest: Environmental and chemical controls. *Biogeochemistry*, *87*(1), 29–47. <https://doi.org/10.1007/s10533-007-9166-3>
- Zimov, S. A., Schuur, E. A. G., & Chapin, F. S. (2006). Permafrost and the global carbon budget. *Science*, *312*(5780), 1612–1613. <https://doi.org/10.1126/science.1128908>
- Zubrzycki, S., Kutzbach, L., Grosse, G., Desyatkin, A., & Pfeiffer, E. M. (2013). Organic carbon and total nitrogen stocks in soils of the Lena River Delta. *Biogeosciences*, *10*(6), 3507–3524. <https://doi.org/10.5194/bg-10-3507-2013>